Calcif Tissue Int (2004) 74:294–301
DOI: 10.1007/s00223-002-1045-2

Calcified Tissue International

Ultrastructure of Dental Enamel afflicted with Hypoplasia: An Atomic Force Microscopic Study

N. Batina,[1] V. Renugopalakrishnan,[2,3] P. N. Casillas Lavín,[4] J. C. H. Guerrero,[4] M. Morales,[1] R. Garduño-Juárez,[5] S. L. Lakka[3]

[1]Departamento de Química, Universidad Autónoma Metropolitana-Iztapalapa, 09340 México DF, Mexico
[2]Children's Hospital, Harvard Medical School, Boston, MA 02115, USA
[3]Department of Biomedical Engineering, Florida International University, Miami, FL 33174, USA
[4]Facultad de Odontología, Universidad Nacional Autonoma de México, 04510 México DF, Mexico
[5]Centre de Ciencias Físicas, Universidad Nacional Autónoma de México, 62210 Cuernavaca, Morelos, Mexico

Received: 10 May 2003 / Accepted: 16 June 2003 / Online publication: 3 November 2003

Abstract. The ultrastructure of the human tooth enamel from a patient diagnosed with hypoplasia (HYP) was investigated using atomic force microscopy (AFM) and compared with the surface of normal human tooth enamel. Hypoplasia is a hereditary defect of dental enamel in which the enamel is deficient in either quality or quantity. AFM results presented for the HYP tooth enamel clearly demonstrate that the apatite crystal morphology in hypoplasia tooth enamel is perturbed in the diseased state which could result from a defective synthesis of the extracellular matrix proteins, e.g., amelogenin, by the ameloblasts. HYP enamel consisting of loosely packed, very small grains does not present a tendency for association, as in the case of the normal healthy tooth. Indeed, the enamel surface affected by HYP is porous and is made of much smaller grains. In some samples, the HYP part of enamel surface appeared in the form of a point-defect, which we believe may be associated with the early stages of the HYP deformation.

Key words: Hypoplasia — Atomic force microscopy — Tooth enamel surface — Surface morphology of tooth enamel — Ultrastructure

Hypoplastic type *amelogenesis imperfecta* (*AI*) represents a group of hereditary disorders that result in defective enamel. The enamel disorders are apparently heterogeneous in their basic structural and chemical defects with a prevalence rate of 1 in 14,000–16,000 reported in the literature [1], depending on the specific type of population. There has been at least one report on the prevalence of enamel hypoplasia in Mexican children [2]. Three major groups of enamel disorders have been classified as *hypoplastic* (thin enamel), *hypocalcified* (primary mineralization defect), and *hypomaturation* (defect in enamel maturation) [3, 4]. The inheritance patterns such as autosomal dominant and recessive, as well as X-linked dominant and recessive, have been reported in the literature [5, 6].

The mineral phase in healthy tooth enamel is comprised of high ordered packing of calcium hydroxyapatite (HA) crystallites, more than ten times larger than those of bones, organized into discrete substructure "prisms" in which the individual crystallites are collectively oriented with their c-axes essentially normal to the plane of the dentino-enamel junction [7].

It is widely accepted that the tissue-specific proteins of the developing dental enamel, amelogenins, provide the extracellular matrix essential for the formation of the unique enamel mineral phase. Amelogenins [8, 9] form a number of protein species that have been isolated, characterized, purified, cloned, and expressed in *E. coli*. The secondary structure of amelogenin has been postulated to orchestrate the mineralization process in enamel. The precise mechanisms underlying the mineralization process are not well understood at the present time. However, it is clear that these unique tissue-specific proteins play a central role in amelogenesis. The secondary structure of bovine amelogenin containing a unique β-spiral structure in the core was derived from circular dichroism (CD) [10], Fourier transform infrared (FT-IR) spectroscopic studies, [11], Raman spectroscopic studies [12] from our laboratory and from molecular mechanics-dynamics refinement from Nuclear Over Hauser (NOE) contacts from 3D NMR studies [13–15]. The 3D structure of bovine amelogenin from multi-nuclear 3D NMR has now been refined (Renugopalakrishnan et al., unpublished data). Recently we have also derived the tentative secondary structure of a more soluble mouse amelogenin, M179, from FT-IR studies (Renugopalakrishnan et al., unpublished data) and its thermal unfolding was investigated using CD

Correspondence to: V. Renugopalakrishnan; E-mail: renu@fiu.edu

and differential scanning calorimetric (DSC) studies (Oobatake et al., unpublished data). The secondary structures of bovine and mouse amelogenin share common secondary structural motifs, despite differences in their primary structures [9]. The absence of polar amino acid residues and the occurrence of a single phosphorylated Ser residue at position 16 suggested that the β-spiral functional domain must derive its Ca^{++} sequestering capability from neutral carbonyl groups of the amino acid residues present in calf amelogenin.

Similar proposals for calcification of tropoelastin have been advanced where the neutral C=O groups are involved in Ca^{++} binding by charge neutralization hypothesis. A cluster of C=O groups aligned on the inner surface of staircase-like structures formed by repetitive β-turns occurring contiguously from Gln-Pro-His-Gln-Pro-Leu-Gln-Pro-His-Gln-Pro-Leu-Gln-Pro-Met-(Gln-Pro-Leu)$_4$, from Gln_{112} through Leu_{138}, offers as an ideal but novel candidate for Ca^{++} binding. The uniqueness of this structure, labeled as β-spiral, and its putative role as Ca++ binding domain occurring between Gln_{112} through Leu_{138}, was the basis for selecting it for detailed molecular mechanics and dynamics studies [13]. Molecular mechanics and dynamics studies revealed a class of dynamic structure for the β-spiral region which could be broadly categorized into β-spiral structure with a ~1 Å diameter pore and one where the pore was blocked by Gln side chains. The ~1 Å diameter pore fits into it us nearly an unhydrated Ca^{++} ion.

The above class of structures are stabilized by 4 β-turn H-bonds and Gln side chain to Gln side chain H-bonds. The hydrophobic side chains are radially projecting outwards with the C=O groups lining the interior symmetrically. Entry of Ca^{++} ions causes a perturbation of the hydrogen bond network and results in a movement of Gln side chains allowing the passage of Ca^{++} ions across the open pore.

Scanning electron microscopic study of hypoplasic type AI in primary teeth was reported by Uzamis et al. [16]. To date, at least three AFM studies of tooth morphology have been reported in the literature [16–18]. There have been at least two reports in the literature of scanning electron microscopic (SEM) studies of the surface characteristics of enamel [18, 19]. We have recently reported the ultrastructure of tooth enamel afflicted by *amelogenesis imperfecta* from our laboratory [20]. The present study is the first report in the literature on the ultrastructure of human tooth enamel from normal patients and patients diagnosed with hypoplasia using atomic force microscopy (AFM).

Materials and Methods

The female patient from whom the HYP tooth was extracted was a patient at the Pedodontic Clinic at the Postgraduate and Research Studies Division, Dental School of the National Autonomous University of Mexico in Mexico City. The sample tooth with HYP was that of the central incisor of the right temporal from a female patient, 10 years 5 months of age, extracted because it was impossible to rehabilitate. The tooth was extracted under local anesthesia and clinically diagnosed by optical microscopic observations. It lacked continuity of enamel and had a marked brownish color with white spots, characteristic of hypoplasia. No family trends were detected, thus it is possible that hypoplasia was developed in the fetal stage of this patient.

Preparation of Human Tooth Enamel and Clinical Diagnosis

The healthy tooth sample, with no dental abnormalities (NA) was from the third lower molar of a 25-year-old male patient. The samples were dissected into small square like plates 1 mm long and 1 mm wide (thickness around 2 mm; the lower side of the sample was polished with carbide fissure burs and disks (SS White, Buffalo, NY, USA) and then cleaned with absolute ethanol. The samples were placed in an ultrasonic cleaner for 5 min and allowed to dry at an ambient temperature. Finally they were fixed on a metal disk (sample holder) with cyanoacrylate adhesive and examined with an AFM microscope.

AFM Studies

The surface morphology of the tooth samples was probed by a commercial Atomic Force Microscope (AFM), Nanoscope III (Digital Instruments, Santa Barbara, CA, USA). Imaging was performed ex-situ (laboratory atmosphere) under controlled temperature and humidity. AFM was operated in "contact" and "tapping" mode (Digital Instruments, manual for Nanoscope III-SPM) [21]. In a simplified manner, these two operational modes differ in terms of physical contact between the AFM probe (tip) and the imaged surface. In the "contact" mode, physical contact between the tooth surface and the AFM tip is maintained at all times with constant force. The three-dimensional motion of the cantilever and the AFM tip attached to the piezo corresponds to the surface morphology of the scanned area. Imaging was performed with standard geometry silicon nitride probes. AFM images were collected at a very slow scan rate of 1 Hz in order to obtain details of the enamel structure and to avoid damaging the tip. The "tapping" mode imaging is a more sophisticated type of measurement, in which the tip contacts the image surface in regular intervals, but does not establish a permanent contact. Tapping mode imaging is recommended for the surface-sensitive type of samples, which could be damaged-during the tip rastering process. Another advantage of the tapping mode imaging is the possibility to collect frequency, amplitude, and phase type of data, which offers complementary information to the surface topography and often gives better lateral resolution. As it is demonstrated in this paper, such extensive and sophisticated AFM analyses have helped us to visualize very fine structural details of different enamel features found at the tooth surface. Shortly before imaging, by both methods, all samples were regularly rinsed with ultra-pure water and dried in a stream of air. We have used an optical stereo-microscope to select five different places for AFM imaging on each sample. Images presented in this paper are mostly plotted in the "height" mode, which is typical for the presentation of surface topography. In this mode the higher part of the surface appears brighter in the 2D or 3D image. The tapping mode data (amplitude and phase imaging) are presented in 2D or "top-view" mode.

Results and Discussion

The observed tooth morphological characteristics are described qualitatively and quantitatively. For

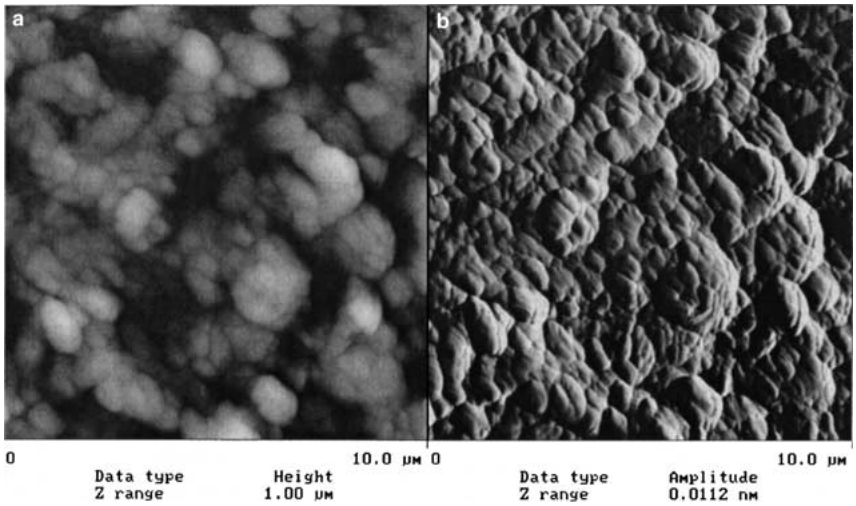

Fig. 1. Top view of AFM tapping mode images of the healthy tooth recorded in "height" (surface morphology) mode (**a**) and "amplitude" mode (**b**). These images clearly reveal the distribution, size, and shape of numerous closely packed grains at the outer enamel surface.

quantitative evaluation, only the "height" mode imaging data and the software package for image analysis, available with the Nanoscope III-AFM instrument, were used. As described before in the experimental part, the surface morphology of the outer part of the human tooth (enamel) has been studied using a normal healthy adult tooth (NA) and a tooth with hypoplasia (HYP-tooth). Each sample was analyzed in terms of surface topography, spatial arrangement, surface roughness, and surface feature characterization, i.e., size and shape of the surface features.

AFM Surface Morphology of the Normal Tooth

In order to learn how to differentiate the major morphological characteristics of the outer surface of enamel for the different samples (healthy and HYP-tooth), we will first focus on characterization of the healthy an tooth from an adult (NA).

AFM images presented in Figures 1a and b show the top surface of the enamel in the NA tooth. Images were collected using the "tapping" technique and presented in "height" (Fig. 1a) and "amplitude" (Fig. 1b) mode. Images recorded in the "height" mode, most frequently used in AFM microscopy, show surface morphology of the imaged area. In these 3-dimensional images, the upper part of the sample is colored brighter (light) than in the lower parts of the surface. Accordingly, one could qualitatively and quantitatively interpret data and characterize such image features (as particle size, shape, height of the observed features). Analysis of our images shows that the tooth surface consists mainly of two kind of grains: small grains (average diameter from 0.2–0.5 micrometers) and large grains (average diameter 2–4 μm). The small grains are incorporated into the large grains. From our images it was difficult to discern any order or some specific grain alignment, however, one could clearly see that grains are in close proximity to each other. In particular, the small grains and their relation to the bigger associates could be clearly recognized in the AFM image recorded in the "tapping" amplitude mode (Figure 1b). This image clearly reveals the compact packing between the apatite grains during the enamel formation. In order to characterize our samples in a more quantitative manner, we also estimated the average surface roughness of the imaged surface for several samples. For NA tooth, the RMS (Rq) (root-mean-square roughness) [22–25], a normal measure used to express the surface roughness, was estimated to be 116.50 nm. The RMS (Rq) value was calculated following a standard procedure previously described in the literature, using the complete AFM image, each of 512 points within each of 512 image lines. Images recorded in the "amplitude" mode, as the one presented in Figure 1b, are not 3D images in terms of surface morphology, and could not be used for evaluation of height of the observed features. However, they reveal more details concerning lateral (in plane) dimension of the imaged object, due to better resolution in x and y directions.

The AFM image in Figure 2 shows a three-dimensional view of the same sample area presented in 1a, b. In such SD-presentation one could clearly recognize HA grains of different size as well as visualize the significance (meaning) of the surface roughness. Note that in this particular image the range of the z scale is about eight times smaller than the x and y scale. In other words, magnification in the z direction is about eight times larger than for x and y. In case of the same presentation scale, with the same magnification for x, y, and z directions, the imaged surface will appear almost flat (featureless).

AFM Surface Morphology Analysis of Tooth Enamel Affected by Hypoplasia

In the present study we have analyzed several hypoplastic teeth collected from adult patients. For each

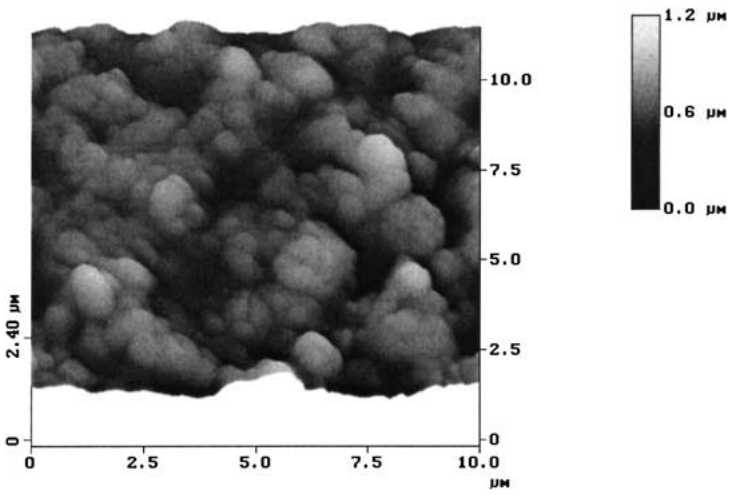

Fig. 2. Three-dimensional presentation of the AFM tapping mode image of the healthy tooth recorded in "height" (surface morphology) mode.

sample, we have scanned at least five different and randomly chosen places. At first we usually scanned a large portion of the sample, 10×10 μm (scanning area of 100 μm^2). Taking into account the total sample size (a square with 1 mm by side) with a total area of 10^6 μm^2 available for scanning, it means that for each height resolution ~0.01% of the surface area was examined. At this point we routinely obtained images similar to those presented in Figure 3 (a and b). These images show the topography at the same location of the tooth surface but one represents a two-dimensional image (Fig. 3a) and the other represents a three-dimensional (Fig. 3b) image. Closely packed, but not organized, grains of small (0.1 to 0.2 μm) and large (associates) size (0.7–0.8 μm) can be observed on the enamel surface. The surface roughness factor was found to be RMS[Rq] = 103.8 nm. The data obtained present characteristics similar to those of a healthy tooth. At this point we realized that the hypoplasia-affected tooth does not necessarily have a homogeneous topography all over the surface, but it seems that hypoplasia affects the tooth over small localized areas. Detailed inspection with a powerful optical stereomicroscope (magnification of 400×) revealed that hypoplasia was causing point type defects on the enamel surface that were difficult to be localized by AFM. As a preliminary step, an area affected by hypoplasia was first localized with the optical microscope and then analyzed by AFM.

To illustrate the morphology of the tooth affected by hypoplasia, we present the AFM image of the tooth surface in Figure 4. It shows the enamel surface partially affected by hypoplasia (the central part of the image). Although the much larger grains (1–1.5 μm) of HA could not be resolved with the height resolution, the part affected by hypoplasia clearly shows different surface texture, as can be observed in the central part of the image. A better resolved image is presented in Figure 5, where the hypoplastic surface consisted of very small (0.05–0.06 μm) HA grains which are loosely associated with the 0.5 μm particles. More importantly, these grains do not show a tendency for close packing and the enamel surface was found to be significantly more porous than the surface of a healthy tooth. Note that in AFM images recorded in height mode the lower part of the surface appears to be of dark contrast. Quantitative analysis from 3D images allows determination of the pore depth. This is one of the major advantages of using AFM instead of classical Scanning Electron Microscopy (SEM).

The diameter of the observed pores was found to be variable; in general, the pore size was between the larger and smaller grains diameters. However, the size of the pores found in between the smallest grains is about the same size as the diameter of these grains. Therefore it seems that the appearance of the pores is related to the missing grains during the enamel formation process. We have also estimated the pore depth to be approximately 8–10 nm. Since most of the surface features (pores and grains) are very small, it is not surprising that the RMS[Rq] for this area was found to be only 18.3 nm. This value is significantly lower than the RMS[Rq] value for the healthy tooth surface. To have a better insight into the difference between these two surfaces, one should also take note of a significant difference in the z-scale between the two sets of images recorded in the height mode. The surface affected by HYP is flat at the nano-scale level. Figure 6 shows the AFM image recorded at the amplitude mode with enhanced clarity and illustrates the difference in the surface texture of the healthy and the hypoplasia-affected tooth surface. This image also emphasize the limited progress (local character) of the hypoplasia deformation as well as highly irregular forms at the enamel surface.

In some cases we have also found enamel surfaces largely affected with hypoplasia. They were found to be uniform, with a large number of small pores and small 50–60 nm grains. In the absence of larger associated grains, the surface roughness had a much lower value in

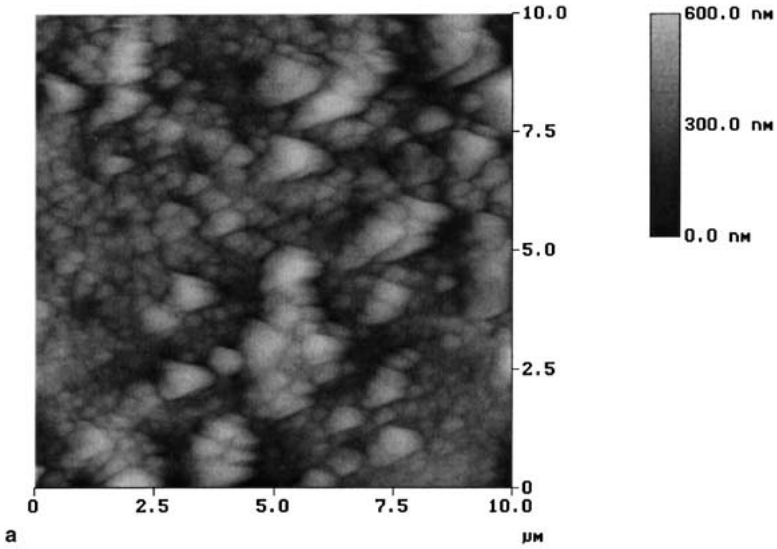

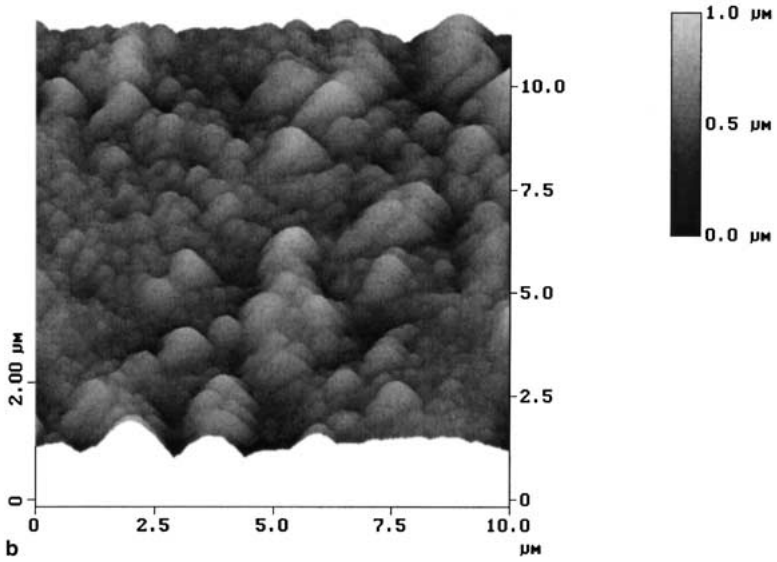

Fig. 3. 3-D presentation of the same AFM images as in Fig. 2., emphasizing the height and topography of the healthy area of the enamel surface.

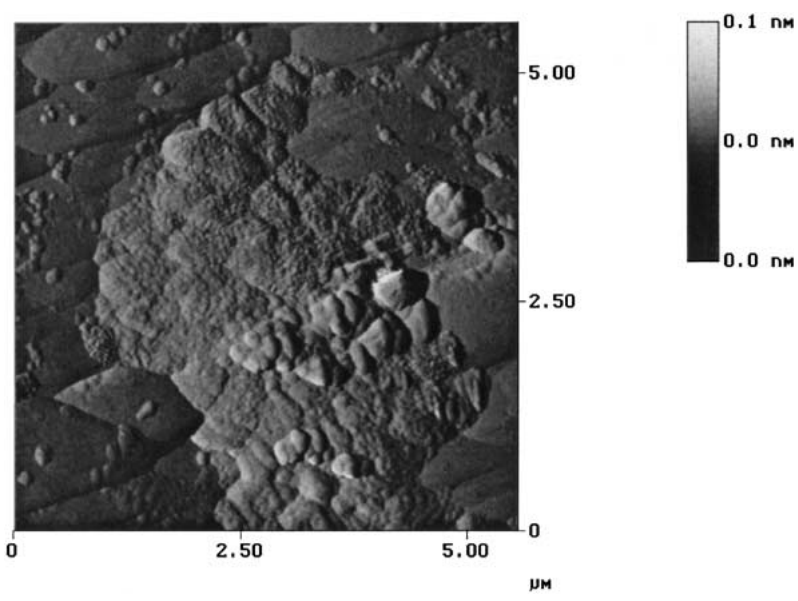

Fig. 4. The AFM image of the tooth surface partially affected by hypoplasia (the central part of the image). Difference in the surface texture of the healthy enamel and part affected by hypoplasia is obvious.

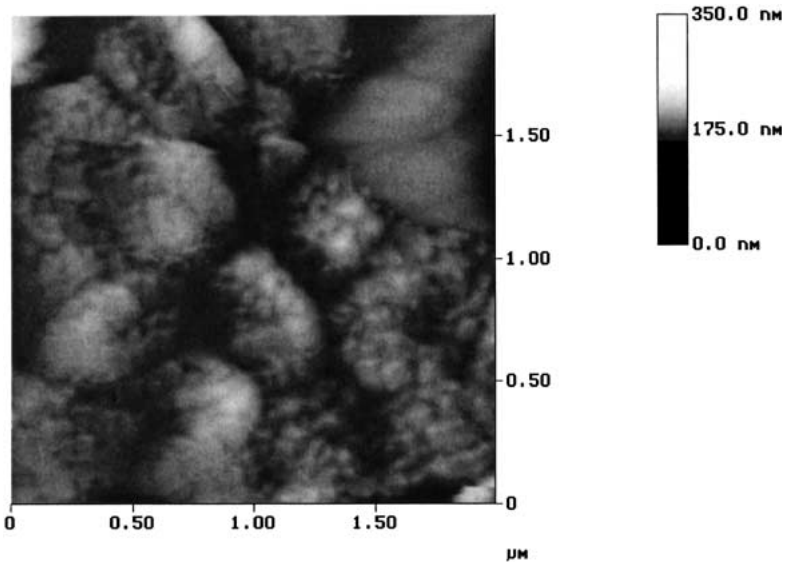

Fig. 5. Top-view AFM tapping mode image of the HYP tooth, recorded in a "height" mode reveals the porous nature of the enamel surface and existence of very small HA grains.

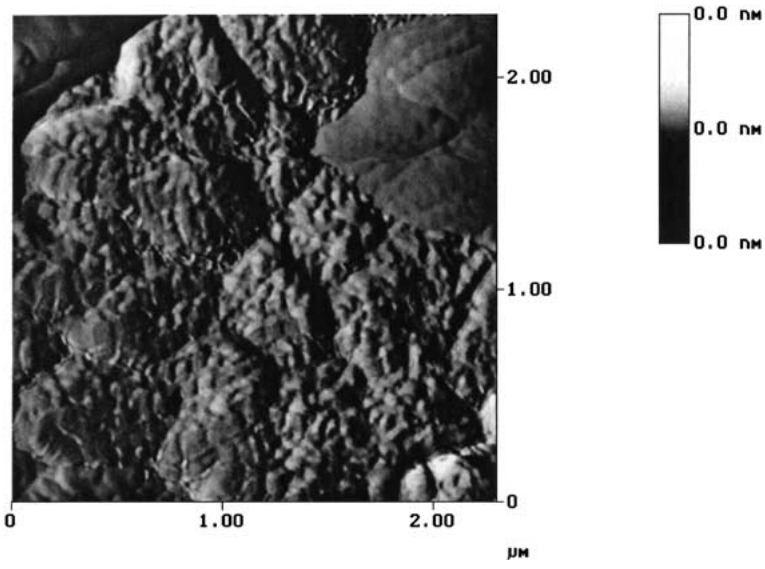

Fig. 6. Details of the HYP tooth structure revealed from the AFM image recorded in the "amplitude" mode, with higher resolution and clarity than one recorded in Fig. 5 in "height" mode.

the nanometer scale, RMS[Rq] = 10 nm. A three-dimensional AFM image of such surface is presented in Figure 7.

Conclusion

AFM visualization of the enamel tooth surface shows significant and distinguishable differences between the ultrastructures of the normal healthy tooth and the one affected by HYP, a significant reduction in RMS [Rq] from 116.5 to 18.3. In the normal healthy tooth the HA is closely packed in the form of large and compact grains. HYP enamel consisted of loosely packed very small grains, which does not present a tendency for association. Indeed the enamel surface affected by HYP is porous, and is made of much smaller grains. It contributes to the height level of smoothness detected as a trait for the HYP surface. In some samples, the HYP part of enamel surface appeared in the form of a point-defect. In others, we found that the entire surface is covered by HYP-type structures. We associate this behavior with HYP deformation progress. In the early stages of the HYP deformation, the appearance of point-defects with HYP surface seems to be the characteristic trait.

According to these morphological findings, one could deduce that the actual influence of amelogenin as a major protein component of the extra cellular matrix is on the development of dental enamel. It is hypothesized that amelogenin acts as an inhibitor during the enamel growth which preferentially forces the formation of isolated apatite grains. Therefore, to study interaction of amelogenin and the enamel surface during the early stages of the biomineralization process will be of special

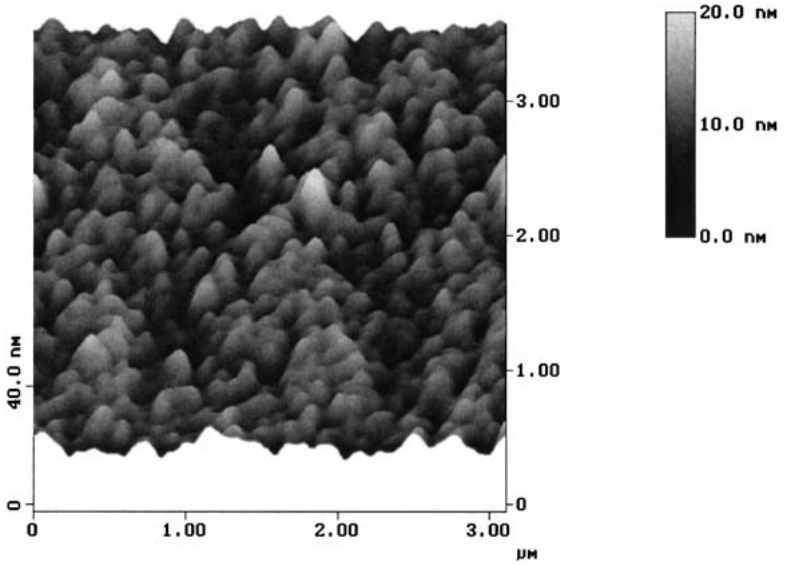

Fig. 7. 3D plot of the AFM image of the HYP tooth recorded in "height" mode, showing the real surface morphology of the enamel outer layer of HYP tooth, with uniformly sized HA grains and pores (missing grains).

interest. From our studies, the molecular mechanism of hypoplasia remains unresolved. The disoriented pattern of hydroxyapatite crystallites seen in the hypoplasia tooth enamel presumably results from altered primary, and hence the secondary structure of extra cellular amelogenin through a cascade of events that are still poorly understood. The secondary structure of human amelogenin has not been reported in the literature. Nevertheless, from the earlier studies of Collier et al. [26], it has been reported that the amelogenin gene responsible for the X-linked AI undergoes the mutation of a conserved Pro $\rightarrow$ Thr and this presumably alters the 3D structure of the human amelogenin. Further studies are in progress in our laboratories that will provide more insight into the molecular basis of hypoplastic type AI. For a better understanding of the molecular mechanisms underlying hypolastic type AI, more detailed visualization of the enamel structure and related proteins will be necessary.

Autosomal dominant amelogenesis imperfecta (ADAI) has been mapped to the long arm of chromosome 4 in three Swedish families [27]. The gene is located in the same region as that involved in dentinogenesis imperfecta as well as genes thought to be involved in enamel development. These genes are the albumin gene and the ameloblastin gene. It is not yet clear whether mutations in these genes are responsible for the ADAI in these families. It seems clear that mutation of the human amelogenin gene is associated with some X-linked types of AI. Our results show that the structure of enamel surface from the healthy tooth and HYP-affected tooth is different and that it can be distinguished by AFM. Indeed, AFM revealed details of the ultra-structure of the enamel surface for both cases, and allows a detailed qualitative and quantitative characterization.

Acknowledgments. This research was partially supported by a grant from the National Institutes of Health (V.R.). V.R. acknowledges partial financial support from CONACyT during 1998–99. N.B. was supported by CONACyT grants, 0913E-P and L0081-E9608.

References

1. Pindborg JJ (1982) Ateiology of developmental enamel defects not related to fluorosis. Int Dent J 32:123–134
2. Goodman AH, Allen LH, Hernandez GP, Amador A, Arriola LV, Chavez A, Pelto GH (1987) Prevalence and age at development of enamel hypoplasia in Mexican children. Am J Phys Anthropol 72:7–19
3. Witkof Jr CJ, Sauk Jr JJ (1976) Heritable effects in enamel. In: Stewart RE, Prescott GH (Eds.) Oral facial genetics. CV Mosby, St. Louis, MO, USA, p 151
4. Witkopf CJ, Rao S (1971) Inherited defects in tooth structure. Birth Defects 7:153–184
5. Backman B, Holmgren G (1988) Amelogenesis imperfecta: a genetic study. Human Hered 38:189–206
6. Shields ED (1983) A new classification of heritable enamel defects and a discussion of dentin defects. Birth Defects 19:107–127
7. Ichio T, Yamashita Y, Terashima T (1992) Observations on the structural features and characteristics of biological apatite crystals. 2. Observation on the ultra structure of human enamel crystals. Bull Tokyo Mod Dent Univ 39:7180
8. Strawich E, Poon PH, Renugopalakrishnan V, Glimcher MJ (1985) Molecular mass determination of major, highest molecular mass extracellular amelogenin of developing bovine enamel. FEBS Lett 184:188–192
9. Fincham AG, Oldalc JM (1995) Recent advances in amelogenin biochemistry. Connect Tissue Res 32:199–124
10. Renugopalakrishnan V, Garduño-Juárez R, Guerrero Juan Carlos Hernández, Patricia N, Casillas Lavin, Ilangovan K (1999) An integrated, holistic experimental and theoretical approach applied to the derivation of 3D structure of bovine amelogenin implicated in amelogenesis imperfecta, a molecular disease characterized by a single point mutation. Rev Quim Mex 43:24–29
11. Renugopalakrishnan V, Strawich ES, Horowitz PM, Glimcher MJ (1986) Studies of the secondary structure of

amelogenin from bovine tooth enamel. Biochemistry 25:4879–4887
12. Zheng S, Tu AT, Renugopalakrishnan V, Strawich E, Glimcher MJ (1987) A mixed β-Sheet and β-turn structure of amelogenin from bovine tooth enamel: Raman spectroscopic evidence. Biopolymers 26:1809–1813
13. Renugopalakrishnan V, Pattabiraman N, Prabhakaran M, Strawich E, Glimcher MJ (1989) Tooth enamel protein, amelogenin, has a probable β-spiral internal channel within a single polypeptide chain: preliminary molecular mechanics and dynamics studies. Biopolymers 28:1823–1833
14. Renugopalakrishnan V, Prabhakaran M, Huang S-G, Balasubramaniam A, Strawich E, Glimcher MJ (1989) Secondary Structure and limited three-dimensional structure of bovine amelogenin. Connect Tissue Res 22:131–138
15. Prabhakaran M, Renugopalakrishnam V, Wilson B, Cheung HC, Strawich E, Glimcher MT (1991) Three-dimensional structure of amelogenin from 2D NMR studies: a molecular dynamics approach. In: Renugopalakrishnam V, Carey PR, Smith ICP, Huang SG, Storer AC (Eds.) Proteins: structure, dynamics, and design. Kluwer Science Publishers BV, Leiden, The Netherlands, p 202
16. Uzamis M, Celik H, Erkmen N, Batirbaygil Y (1997) Scanning electron microscopic study of hypoplastic type amelogenesis imperfecta in primary teeth. J Clin Pediatric Dentistry 21:265–268
17. Kinney JH, Baldouch M, Marshall GW, Marshall SJ (1993) Atomic force microscopy study of dimensional changes in human dentine during drying. Arch Oral Biol 38:1103–1107
18. Aldred MJ, Crawford PJM, Rowe W, Shellis RP (1992) Scanning electron microscopic study of primary teeth in X-linked Amelogenesis Imperfecta. J Oral Pathol Med 21:186–192
19. Backman B, Anneroth G, Horstedt P (1989) Amelogenesis Imperfecta, a scanning electron microscopic and microradiographic study. J Oral Pathol Med 18(3):140–145
20. Batina N, Renugopalakrishnan V, Lavin NC, Guerrero JCH, Morales M, Garduño-Juárez R (2002) An atomic force microscopic study of the ultrastructure of dental enamel afflicted with Amelogenesis Imperfecta. J Biomaterial Sci Polymer 13:337–348
21. Maganov SN, Whangbo M-H (1994) Surface analysis with STM and AFM. VCH, Weinheim
22. McDermott MT, McDermott CA, McCreery RL (1993) Scanning transmission microscopy of carbon surfaces: relationship between electrode kinetics, capacitance, and morphology for glassy carbon electrodes. Anal Chem. 65:937–944
23. Phillips RJ, Golden TD, Shumsky MG, Switzer JA (1994) Evolution of crystallinity during the electrodeposition of body-centered cubic thallium (III) oxide onto glossy carbon. J Electrochem Soc 141:2391–2402
24. Aubach D, Cohen Y (1996) The application of atomic force microscopy for the study of li deposition processes. J Electrochem Soc 143:3525–3532
25. Li YG, Lasia A (1997) Study of gold deposition on copper by electrochemical and microscopic techniques. J Appl Electrochem 27:643–650
26. Collier PM, Sauk JJ, Rosenbloom J, Yuan ZA, Gibson CW (1997) An amelogenin gene defect associated with human X-linked Amelogenesis Imperfecta. Arch Oral Biol 42:235–242
27. Forsman K, Lind L, Backman B (1994) Localization of a gene for autosomal dominant amelogenesis imperfecta (ADAI) to chromosome 4q. Hum Mol Genet 3:1621–1625